MOLECULAR PHYSICS, 1984, VOL. 52, NO. 3, 541–566

An investigation of the laser optogalvanic effect for atoms and molecules in recombination-limited plasmas

by JÜRGEN PFAFF, MARIANNE H. BEGEMANN and RICHARD J. SAYKALLY

Department of Chemistry, University of California, Berkeley, California 94720, U.S.A.

(*Received* 24 *November* 1983 ; *accepted* 28 *January* 1984)

In this paper the nature, the characteristics, and the potential applications of the optogalvanic effect are explored in a broad set of experiments. The optogalvanic effect was investigated, for the Ar, Ne, He, Ar^+, He^+, Cu and Na atoms and N_2, H_2, CO, CN, NH_2, He_2, and CuO molecules in recombination-limited hollow cathode plasmas, with the use of dye lasers. Comparative studies of the time dependence of transitions from metastable and non-metastable states of neutrals and non-metastable states of ions were made. Autoionizing transitions in Cu(I) were found to yield very strong OGE signals. An examination of the various processes known to be important in such plasmas indicates that associative ionization is a very effective means for coupling light energy into the plasma. Measurement of Rydberg transitions in the helium dimer suggests that optogalvanic spectroscopy in recombination plasmas may be useful as a way to study such molecules with repulsive ground states by generating them ' from the top down ' by recombination.

1. INTRODUCTION

The optogalvanic effect (OGE), in which intense light from a laser is used to induce current or voltage changes in a plasma, has recently been exploited for a number of purposes, including analytical flame spectroscopy [1], laser stabilization [2], plasma diagnostics [3], atomic spectroscopy [4] and most recently, molecular spectroscopy [5], and dynamics [6]. The generality of the OGE is evidenced by the facts that four different types of plasma sources have been utilized for these studies, viz. flames [1], positive column DC discharges [2–4], hollow cathode DC discharges [4] and radiofrequency discharges [5], that lasers operating throughout the visible and infrared have been employed as radiation sources, and that both resonant transitions and broadband non-resonant background signals are observed.

The mechanism of the OGE has generally been thought to involve laser enhancement of the ionization rates of atoms or molecules present in the plasmas or a laser-induced depletion of the populations in metastable excited electronic states [6]. Several models of the OGE have been constructed, each appropriate for a given type of plasma. However, these are principally phenomenological in nature and do not account for many of the complex processes occurring in ionized gases that could, in principle, be involved in a laser-induced impedance

change. Particularly, the mechanisms responsible for the OGE observed with infrared lasers may not be the same as those that are important at visible frequencies.

We have previously reported the observation of infrared optogalvanic spectra obtained near 2·7 μm using a colour centre laser [7]. Transitions originating in low-lying Rydberg states of neon, argon, lithium, and barium atoms, generated in commercial hollow cathode lamps, and of hydrogen and helium atoms, generated in a planar hollow cathode (PHC), were observed in this preliminary work. In this paper we present the results of a study in which the OGE was used to obtain electronic spectra of a variety of atoms and molecules in the PHC and in a slotted hollow cathode (SHC) using pulsed and cw dye lasers operating at visible wavelengths. In addition, we report the first definitive detection by this method of atomic ions having high second ionization energies (He^+, Ar^+).

The objective of this research was to explore the potential of recombination-limited hollow cathode discharges for optogalvanic spectroscopy of atoms, molecules, and ions. In particular, electron–ion recombination can dominate the plasma loss mechanisms in these types of discharges ; since this process can be state-selective, the OGE in a hollow cathode plasma could provide a sensitive new detection technique for laser-induced electronic transitions in molecular ions. Furthermore, since electron–ion recombination can produce the corresponding neutral species in a high Rydberg state, which then relaxes by radiating and/or predissociating, the OGE in a recombination-limited plasma offers the prospect of carrying out spectroscopic studies of neutral molecules generated ' from the top down ', i.e. by forming the molecules in high Rydberg states through recombination. Such a scheme could prove valuable for investigating the electronic structures of molecules for which the corresponding positive ions are stable, but whose own ground states are repulsive (e.g. H_3, NH_4, H_3O, He_2, Ne_2, HeH and ArH), particularly because optogalvanic spectroscopy can be a sensitive means of monitoring predissociation channels in such systems and would therefore be complimentary to emission studies, such as those recently conducted by Herzberg and his collaborators on H_3 [8] and NH_4 [9].

2. Experimental

A block diagram of the OGE apparatus is given in figure 1. Pulsed laser radiation was generated with a flashlamp pumped dye laser (Chromatix CMX-4) and cw radiation by a ring dye laser (Spectra-Physics 380-C) pumped with either an argon or krypton ion laser (Spectra-Physics 171), all rented from the San Francisco Laser Center. The operating parameters of these lasers are summarized in table 1. The wavelength of the visible laser radiation was determined by coupling a fraction of the power into a commercial hollow cathode lamp filled with neon and recording the neon optogalvanic spectrum along with that from the hollow cathode discharge generating the plasma being studied. The laser beam was directed through either the PHC or the SHC with from one to 12 passes. The pulsed laser could be focused in order to achieve multipassing, however, the focusing itself had no noticeable effect on the parameters of the OGE signal. The HC discharges were driven by a regulated DC supply with a ballast resistor inserted in series. Laser induced impedance changes in the

plasma were detected by monitoring the discharge current through an additional series resistor (100 Ω) or by directly monitoring the voltage across the discharge itself. The OGE signal was ac coupled (10 nF) into a boxcar averager (PAR162/164) or a lock-in amplifier (PAR124A) and displayed on a two channel strip chart recorder along with the neon calibration spectrum.

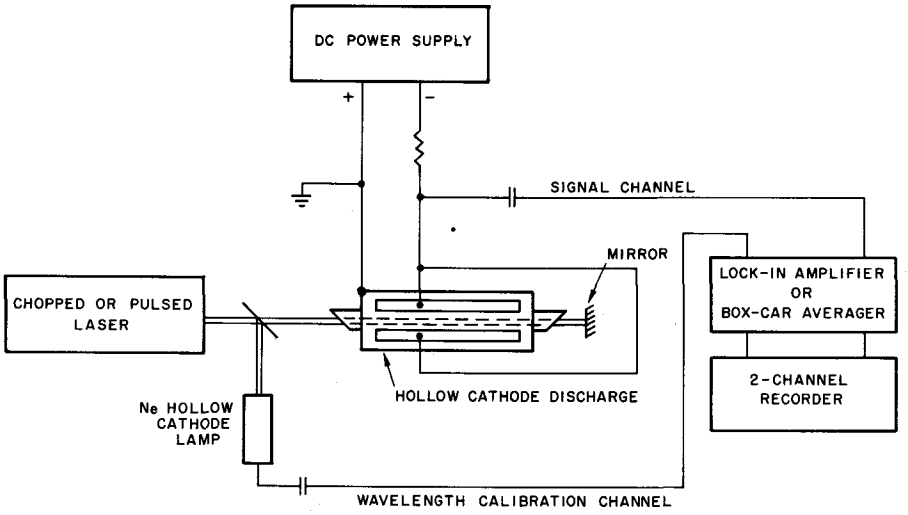

Figure 1. Schematic diagram of the optogalvanic spectroscopy experiment.

Table 1. Operating parameters of the laser systems.

Laser system	Pulse width	Peak power	Average power	Line width	Repetition rate
Flashlamp pumped dye laser (Chromatix CMX-4)	1 μs	3·3 kW	100 mW	3 cm^{-1}	30 Hz
Ring dye laser (Spectra physics 171/380c)	*	*	500 mw	0·1 cm^{-1}	cw

Diagrams of the hollow cathode systems used in this work are presented in figure 2. The PHC design is essentially that used for the gain cell of a copper vapor laser by Warner *et al.* [10]. It consists of two 10 cm long pieces of copper X-band waveguide (1·3 × 2·5 cm) that are mounted in parallel in an aluminium anode block. Water cooling of the cathodes is achieved through the use of 0·75 cm diameter copper tubes which pass through the anode block. These are also used to make electrical connections to the cathodes. Isolation of the cathode feedthroughs from the anode is achieved with the use of teflon mounts and o-ring seals. The ends of the waveguide are sealed with silver-soldered strips of copper to allow for the water cooling. The separation of the cathodes is adjustable from 0·5 cm to 1·5 cm. Aluminium spacers are placed between each cathode and the aluminium anode so that the distances between the copper cathodes and the

anode block are kept small enough ($\leqslant 1$ mm) to prevent the occurrence of a discharge in the gap between them. In the SHC configuration the slot that confines the discharge is bored into a 10 cm long copper cathode, with a cross section of $0{\cdot}7 \times 0{\cdot}7$ cm. An opposing planar copper anode is placed $\leqslant 1$ mm away from the cathode, confining the negative glow discharge to the slot region. The copper anode and slotted cathode are both hollow to allow for water cooling, and are mounted into the aluminium block with teflon seals, electrical connections, and water feedthroughs similar to those used for the PHC.

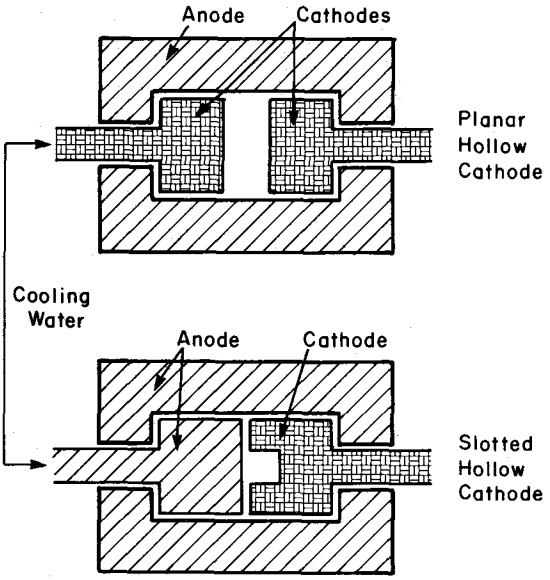

Figure 2. Cross-sections of the hollow cathode discharge cells used in this work. Top: Planar hollow cathode (PHC), as described by Warner *et al.* [10]. Bottom: Slotted hollow cathode (SHC)

In the PHC plasma the surface of each cathode is covered with a thin luminous glow (cathode glow) which is bounded by a dark space (cathode sheath) about 1 mm thick. The region between the two dark spaces (the negative glow) is sampled by the laser beam. With the geometry of this discharge, the positive column is normally suppressed. The properties of a PHC plasma have been rather thoroughly investigated for the case of pure helium at both high and low current densities and for pressures in the range 4–8 torr [11]. In pure helium, nearly all (~ 99 per cent) of the discharge potential (200–600 V) appears across the cathode sheath regions. Ionization in the negative glow is maintained primarily by 'beam electrons'; these electrons are produced by bombardment of the cathode surfaces with positive ions, photons, and metastable atoms and are accelerated through the cathode sheath to energies approaching the full cathode fall (~ 200 V). These electrons, as well as secondary electrons produced by ionizing collisions of beam electrons with the background gas, are trapped between the sheath potentials and degrade in energy by elastic and inelastic collisions until the majority of electrons thermalize to approximately

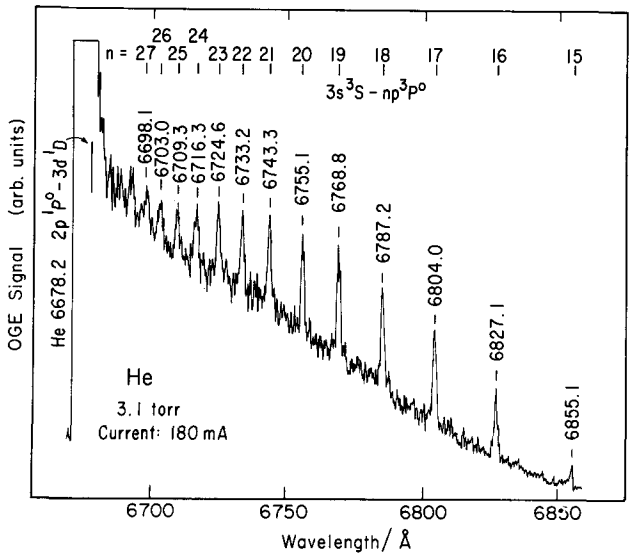

Figure 3. A He Rydberg series originating in $3s\,^3S$ to $np\,^3P^0$ is observed near the red wing of the strong 6678·2 Å He line. The broadening of high-n lines is caused by the plasma Stark effect (Holtzmark theory [12]).

$\sim 0{\cdot}7$ eV (~ 900 K). The electron and ion densities in the negative glow plasmas can exceed 10^{13} cm^{-3} for current densities of 0·01 A cm^{-2} and vary approximately linearly with current. An estimate of the electron density in these studies was made possible by the measurement of the He $3s\,^3S$ to $np\,^3P$ Rydberg series, obtained with the CMX-4 laser system (figure 3). Transitions to levels with n as large as 27 are clearly distinguishable, while higher members are obfuscated by the very strong He $2p\,^1P_0$–$3d\,^1D$ transition. Stark broadening of the high-n lines is clearly discernible. The Stark-broadened linewidth for high principal quantum numbers can be approximately related to the plasma density by Holtzmark theory [12] whence

$$\Delta\lambda = \frac{\lambda_0^2 Z_p h}{\pi c Z M_e}(n_f^2 - n_i^2) N_p^{2/3}, \tag{1}$$

where Z and Z_p represent the nuclear charge of the radiator and perturber respectively, λ_0 is the resonance wavelength and N_p is the sum of electron and ion densities, which are assumed to be equal. Since the Stark-broadened linewidth increases with both electron density and n, high-n levels can only be observed at low electron densities. From the linewidths of the $3s\,^3S$–$np\,^3P$ series, we estimate an electron density (n_e) of $1\text{–}2 \times 10^{11}$ cm^{-3} in helium, using rather mild discharge conditions ($I = 0{\cdot}15$ A, cathode spacing $= 1{\cdot}0$ cm, $P = 3$ torr, $J = 0{\cdot}003$ A cm^{-2}), which allowed for the observation of high n levels and thus enabled us to set a lower limit on the electron density under these conditions. By scaling to the higher pressures and current densities of the slotted cathode (0·024 A cm^{-2}) we estimate considerably higher electron densities, approaching 2×10^{13} cm^{-3}. Because of the combination of a high plasma density and a very low electron

temperature in these discharges, both radiative electron-ion recombination and three body recombination are important loss mechanisms for the charged particles, along with ambipolar diffusion. When operated at appropriate pressures and currents, the plasma can be extremely quiet and stable. These characteristics of high plasma density, low plasma temperature, and very stable, noise-free operation make these special hollow cathode plasmas attractive for optogalvanic spectroscopy of molecules.

Although the slotted hollow cathode has not been modelled in the same detail as the PHC, its characteristics are known to be very similar [11]. Due to the smaller cathode surface area the current density is higher and because of the smaller volume the discharge operates at a higher pressure, typically between 5 and 10 torr. The largest OGE signals were found with the slotted cathode configuration. In this configuration there is a much better overlap of the laser beam with the discharge. Consequently, the laser-perturbed portion of the discharge carries a correspondingly larger fraction of the total current.

3. Results

Using the flashlamp-pumped dye laser and the cw ring dye laser systems, electronic spectra of Ar, He, Ne, Ar^+, He^+, Cu and Na atoms (table 2) and of the N_2, H_2, CO, CN, NH_2, He_2, and CuO molecules (table 3) were observed. Current, pressure, and time dependence of the atomic OGE signals were measured.

3.1. *Atomic spectra*

The extensive spectra observed for neutral argon, neon, and helium atoms, originating in both metastable and non-metastable levels, were used primarily to probe the conditions in the hollow cathode plasmas. Laser-enhanced ionization was generally believed to be the mechanism for the OGE involving non-metastable states. Ionization of laser-excited atoms or molecules occurs principally through collisions with other excited species or with thermal electrons. In argon the upper levels of the observed OGE transitions are 2100–5100 cm^{-1} below the lowest Ar^+ state. The laser excitation thus transfers the Ar atom from an initial state lying > 25 kT below ionization by thermal electrons to a state which lies from 3 to 5 kT from ionization. The laser excitation therefore greatly increases the number of electrons that are capable of ionizing the atoms. In contrast, we have observed Ar^+ transitions in which the upper states lie 60 000 cm^{-1} below the next ionization potential. In this case the excited species is still more than 80 kT below the ionization potential, with respect to thermal electrons, such that laser enhancement of ionization by collisions with thermal electrons can clearly be excluded as an important mechanism for the OGE. While for other species studied by OGE the situation is intermediate between these extreme cases, it is clear that mechanisms other than laser enhanced ionization must be considered to be of general importance for OGE transitions from non-metastable levels.

The most intense Cu(I) transitions observed were those terminating in states above the lowest ionization potential, and which therefore exhibit autoionization [13]. These transitions, in which the laser excitation directly increases the number of electrons in the discharge (autoionizing lifetime of $\leqslant 10$ ps), are

Table 2. Atomic transitions observed.

Species	Transition	Air wavelength/Å	Comment
He I	$2s\ ^1S$–$3p\ ^1P^0$	5015·7	Metastable lower state
He I	$2s\ ^1S$–$7p\ ^1P^0$	3355·5	Metastable lower state
He I	$2s\ ^1S$–$8p\ ^1P^0$	3297·7	Metastable lower state
He I	$2p\ ^1P^0$–$3d\ ^1D$	6678·2	Short lived (<1 ns) lower state
He I	$2p\ ^1P^0$–$4d\ ^1D$	4921·9	Short lived (<1 ns) lower state
He I	$2p\ ^1P^0$–$4s\ ^1S$	5047·7	Short lived (<1 ns) lower state
He I	$2p\ ^3P^0$–$3d\ ^3D$	5875·6	Short lived (<1 ns) lower state
He I	$3s\ ^3S$–$np\ ^3P^0$	6698·1–6855·1	$15 \leqslant n \leqslant 27$ Rydberg Series
He II	$n=4$–$n=6$	6560	19 lines within 0·7 cm^{-1}
Ar I	$4p$–$6s$		
Ar I	$4p$–$7s$		
Ar I	$4p$–$8s$		
Ar I	$4p$–$6d$		
Ar I	$4p$–$7d$		
Ar I	$4p$–$4d'$		
Ar I	$4p$–$5d'$		
Ar I	$4p$–$6s'$	5650–6690	~70 lines
Ar I	$4p$–$7s'$		
Ar I	$4p'$–$5d'$		
Ar I	$4p'$–$7s'$		
Ar I	$4p'$–$8s'$		
Ar I	$4p'$–$7s$		
Ar I	$4p'$–$8s$		
Ar I	$4p'$–$5d$		
Ar I	$4p'$–$6d$		
Ar I	$4p'$–$7d$		
Ar II	$3d\ ^4F_{9/2}$–$4p\ ^4D_{7/2}^0$	6643·7	
Ar II	$3d\ ^4F_{7/2}$–$4p\ ^4D_{5/2}^0$	6684·3	
Ar II	$3d\ ^4F_{5/2}$–$4p\ ^4D_{3/2}^0$	6638·2	
Ar II	$3d\ ^4F_{3/2}$–$4p\ ^4D_{1/2}^0$	6639·7	Upper states of the transitions lie
Ar II	$3d\ ^2P_{1/2}$–$4p\ ^2P_{1/2}^0$	6666·4	more than 60 000 cm^{-1} below the
Ar II	$3d\ ^2P_{3/2}$–$4p\ ^2S_{1/2}^0$	6483·1	2nd *IP*
Ar II	$3d\ ^2P_{1/2}$–$4p\ ^2S_{1/2}^0$	6103·6	
Ar II	$3d\ ^4F_{5/2}$–$4p\ ^2D_{3/2}^0$	6138·7	
Cu I	$4s\ ^2S_{1/2}$–$4p\ ^2P_{3/2}^0$	3247·5	
Cu I	$4s\ ^2S_{1/2}$–$4p\ ^2P_{1/2}^0$	3274·0	
Cu I	$4s^2\ ^2D_{3/2}$–$4p'\ ^2F_{5/2}^0$	3279·8	
Cu I	$4s^2\ ^2D_{5/2}$–$4p\ ^2P_{3/2}^0$	5105·5	
Cu I	$4s^2\ ^2D_{3/2}$–$4p\ ^2P_{1/2}^0$	5782·1	
Cu I	$4p\ ^2P_{1/2}^0$–$4d\ ^2D_{3/2}$	5153·2	
Cu I	$4p'\ ^2F_{5/2}^0$–$5s'\ ^4D_{3/2}$	5034·4	Autoionizing upper state
Cu I	$4p'\ ^2F_{7/2}^0$–$5s'\ ^2D_{5/2}$	5076·2	Autoionizing upper state
Cu I	$4p'\ ^4D_{7/2}^0$–$5s'\ ^4D_{5/2}$	5144·1	Autoionizing upper state
Cu I	$4p'\ ^2P_{3/2}^0$–$5s'\ ^2D_{3/2}$	5158·4	Autoionizing upper state
Cu I	$4p'\ ^2F_{5/2}^0$–$5s'\ ^4D_{5/2}$	5200·9	Autoionizing upper state
Cu I	$4p'\ ^4D_{5/2}^0$–$5s'\ ^4D_{3/2}$	5212·8	Autoionizing upper state
Cu I	$4p'\ ^4D_{3/2}^0$–$5s'\ ^4D_{3/2}$	5250·5	Autoionizing upper state
Na I	$3s\ ^2S_{1/2}$–$3p\ ^2P_{3/2}^0$	5890·0	
Na I	$3s\ ^2S_{1/2}$–$3p\ ^2P_{1/2}^0$	5895·9	

Table 3. Molecular transitions observed.

Species	Laser mode	Transition	(v', v'')	Air wavelength/Å	Comment
N_2	cw + Pulsed	$B\,^3\Pi_g$–$A\,^3\Sigma_u^+$	$\Delta v = 4$ progression $v'' = 0$–6	5845–6190	
	cw		(13, 10)		Upper state predissociated
	cw	$c_4\,^1\Pi_u$–$a''\,^1\Sigma_g^+$	(0, 0)	5960–6000	Ledbetter band
NH_2	cw	$^2A_1$–$^2B_1$	(0, 9, 0–0, 0, 0) Σ, Δ, Γ subbands (0, 10, 0–0, 0, 0) Π, Φ subbands (1, 6, 0–0, 0, 0) Φ subband	5700–6200	Generated from $N_2 + H_2$ In discharge
H_2	Pulsed	$i\,^3\Pi_g$–$c\,^3\Pi_u$	(0, 0) (1, 1) (2, 2)	5830–6050	Very weak
CuO	cw	$A\,^2\Sigma^+$–$X\,^2\Pi_{3/2,1/2}$	(0, 0) (1, 1)	6059–6165	Metal sputtered from cathode
He_2	cw	$f\,^3\Sigma_u^+$–$b\,^3\Pi_g$	(0, 0)		
	cw	$f\,^3\Pi_u$–$b\,^3\Pi_g$	(0, 0) (1, 1)	5680–6050	Repulsive ground-state
	cw	$f\,^3\Delta_u$–$b\,^3\Pi_g$	(0, 0) (1, 1)		
CO	Pulsed	$d\,^3\Delta_i$–$a\,^3\Pi_r$	(3, 0) (4, 1) (7, 0)	6380–6670 5030–5145	
CN	Pulsed	$A\,^2\Pi$–$X\,^2\Sigma^+$	(7, 2) (8, 3) (9, 4) (4, 0) (6, 2) (7, 3) (8, 4)	5480–6220 6400–6820	Generated from C_2N_2 in discharge

perhaps the optimum type of resonant transitions for detection by the OGE. It has been noted [14] that lines originating in autoionizing states can only be observed in arc emission spectra above a minimum current of ~ 1 A, and that these lines increase in intensity with both arc current and pressure, whereas the sharp, non-autoionizing lines do not exhibit this behaviour. This indicates that the rate of ion-electron recombination, which produces the autoionizing states, has to be high enough to rival the autoionization rate in order for emission to be detectable from such autoionizing states. In emission these autoionizing lines are, for obvious reasons, much weaker than the non-autoionizing lines. In OGE, however, the situation is exactly reversed ; the autoionizing transitions

are $\sim 10^3$ more intense than the non-autoionizing transitions. The linewidths of these transitions are 5–10 cm^{-1}, noticeably broader than non-autoionizing transitions. This suggests that accurate linewidths obtained from OGS could be a means for measuring picosecond autoionizing rates, which are difficult to measure by emission spectroscopy because of pressure and Stark broadening. Such measurements were not attempted in this exploratory work, since the linewidth was limited by the laser bandwidth (3 cm^{-1}). The similar utilization of linewidths of optogalvanic transitions to measure picosecond predissociation rates of the HCO radical has recently been demonstrated by Vasudev and Zare [15].

The largest resonant OGE signals observed in this work (> 1 V_{pp}) were those from the He $2p$–$3d$ singlet transition at 5875 Å and the $2p$–$3d$ triplet transition at 6678 Å.

We estimate that, given the noise levels in these experiments (0·3 μV), a relative absorption of 5×10^{-7} can be detected, assuming the same efficiency of this He transition for producing an impedance change. It is interesting to note that these particular transitions neither originate in a metastable level nor terminate in a high Rydberg state, and therefore would not be expected *a priori* to be an optimum candidate for detection by OGE. As we discuss later in the paper, the opening of very efficient associative ionization channels is responsible for these extraordinarily strong signals.

In figure 4 the current and pressure dependences of the Ar(I) $4p[1/2]1$–$6s[1/2]^0 0$ and $4p[5/2]3$–$7s[3/2]^0 2$ transitions at 5882·6 and 5888·6 Å, respectively, are shown. Both transitions increase in intensity with increasing current, albeit somewhat irregularly. The reason for such an irregular variation is the simple fact that the PHC cannot be operated over a continuous range of currents without effecting a change in the plasma mode ; hence it is difficult to establish more than a general trend. The increase of OGE signals with current is a very general behaviour and is most likely the result of increasing the population in the lower level of the transition due to both inelastic electron–atom collisions and electron–ion recombination processes, the rates of which increase with the plasma density. Furthermore, all of the neutral species studied here yielded more intense signals at small cathode spacing due to the same effect, viz. increased plasma density.

The pressure dependences of the OGE signals vary with the particular species and states observed. In figure 4 it is clear that the two argon transitions originating from states differing only by the values of the j–l coupling, and separated in energy by 1360 cm^{-1}, have completely different pressure dependencies. The $4p[\frac{1}{2}]1$ to $6s[1/2]^0 0$ transition exhibits no pressure dependence over the range between 1·5 and 5 torr. The lower state of the transition has the least energy of all the states with the excited electron in a $4p$ orbital. The energy difference between the lowest state in the $4p$ manifold to the next higher state is 1360 cm^{-1}. Excitation of the higher state in collisions with He therefore is hampered by a Boltzmann factor of $\sim 1{\cdot}5 \times 10^{-3}$ as compared with quenching of the higher state. Collisional quenching could only occur to states with different orbital or different principal quantum numbers. The cross section for such quenching processes is clearly too small to be observed at the pressures employed here. The transition $4p[5/2]3$–$7s[3/2]^0 2$ decreases approximately linearly with increasing pressure, however, indicating a rapid quenching of the lower level to the

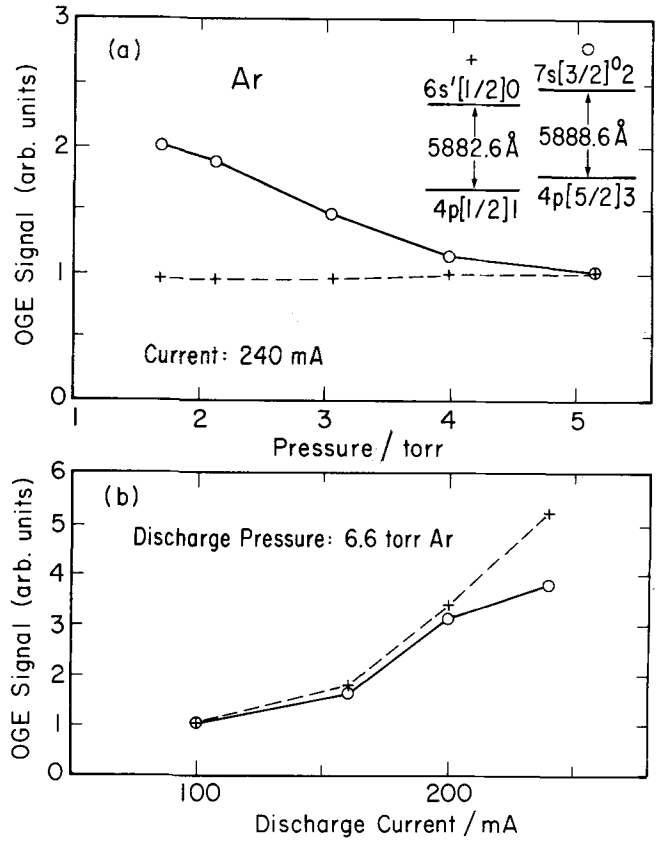

Figure 4. Pressure (*a*) and discharge current (*b*) dependences of the optogalvanic signals for two different Ar lines.

lowest state of the 4*p* manifold. A decrease of the OGE signal with pressure is the type of behaviour most frequently noted for transitions studied here. Collisional quenching is known to decrease the populations in highly excited electronic states of atoms and molecules quite efficiently at the pressures used in this experiment (several torr). As a result, one would generally expect OGE signals that originate in such levels to decrease with pressure.

Evidence for the importance of highly excited electronic states in maintaining the discharge is obtained from the fact that continuous background signals were observed in all the laser OGE spectra, and that they increased dramatically at low pressures. Direct laser ionization (bound-free transitions) of highly excited states, which are quenched at higher pressure, is most probably the source of this background. Anomalously large non-resonant OGE signals were observed when the pulsed dye laser output was focused onto the cathode surface. Laser-induced voltage decreases as large as 180 volts (90 per cent of the total discharge voltage) were measured for helium at wavelengths around 6500 Å. Hence, the discharge impedance could essentially be switched to zero with a laser pulse. We attribute these large surface effects to laser vaporization of carbon, which was deposited on the cathode surface while running a discharge in He/CO or He/C_2N_2(100 : 1) mixtures. Vaporization of carbon by the focused

laser pulse produces a cloud of carbon atoms with high density above the cathode surface. The ionization potential of carbon is significantly lower than that of He (11·3 eV versus 24·6 eV). Therefore a high density cloud of carbon ions is produced close to the cathode surface shortly after the laser pulse, essentially causing the discharge to ' arc '. The carbon ions are then accelerated into the cathode surface and are redeposited, extinguishing the arc. The small cathode surface area exposed to the laser slowly gets cleaned, and as a result we observe a decrease of this surface effect with a time constant of seconds or minutes, depending on the history of the cathodes.

In previous studies of the OGE, spectra of several atomic ions have been detected; of these Eu^+, Ba^+ [16], and U^+ [17] have quite low second *IP*s (11·25 and 10·00 eV respectively, IP_2 of U is not available) while the spectra attributed to I^+ are tentative assignments [18]. The fact that electron–ion recombination is a major loss mechanism for ions and electrons in the PHC plasma suggests a general mechanism for the detection of optogalvanic spectra of ions formed in this environment, viz. laser-induced changes in their recombination rates. In order to examine this possibility, OGE spectra of He^+ ($IP_2 = 438\ 909\ cm^{-1}$) and Ar^+ ($IP_2 = 222\ 848\ cm^{-1}$) were studied. As indicated in table 2, the unresolved $n = 4$ to 6 transitions in He^+ and eight transitions in the $3p^4\ 3d$–$3p^4(^3P)^4P$ series in Ar^+ were observed. All of the ionic lines were found to increase in intensity with increasing current and to decrease in intensity with increasing pressure. The ion signals maximized at the largest possible cathode spacing (1·5 cm). This supports the contention that it is a laser-induced change in recombination rate of the ions with electrons that is responsible for the signals. Increasing the cathode spacing has the effect of decreasing the diffusion losses of ions and thus enhances the relative importance of ion–electron recombination.

In figure 5 the time dependence of (*a*) metastable He($2s\ ^1S$–$2p\ ^1P$) vs non-metastable He($2p\ ^1P_0$–$4s\ ^1S$) and (*b*) ionized He ($n = 4$–$n = 6$) vs neutral He($2p\ ^1P_0$–$3d\ ^1D$) are compared. All of these signals exhibit at least one positive and one negative portion, indicating that at least two different processes are involved in the OGE. The OGE signal originating in a radiatively metastable level of He(I) consists of a strong positive part (increase in discharge current) peaking at about 4 μs, followed by a strong negative part (decrease in discharge current) peaking at ~ 7 μs, and a weak long time positive part maximizing at ~ 15 μs. By comparison, a He(I) signal originating in a non-metastable (short-lived) level possesses a slightly earlier strong positive-going part and a much weaker and slightly later negative part. The $n = 4$ to 6 transition of He^+ exhibits a time dependence very similar to that of the non-metastable He(I) transition, but the early positive part of the signal is much broader and occurs about 0·5 μs before that of He(I), while the late negative part occurs at the same position as that of He(I). Due to the markedly different time dependences of Ar^+ and He^+ compared to neutral Ar and He it was possible to effectively separate ionic from neutral spectra by setting the gate of the boxcar averager at different delay times (figure 6). This proved to be a powerful advantage in studying the ionic OGE signals. The time-resolved non-resonant background signals exhibited the same characteristic voltage changes as the resonant ones, however, with a different magnitude. The initial fast positive portion of the signal occurred within ~ 1 μs of the laser pulse, followed by a negative portion at 2–3 μs. A long positive tail extending to 50 μs of the laser pulse and peaking

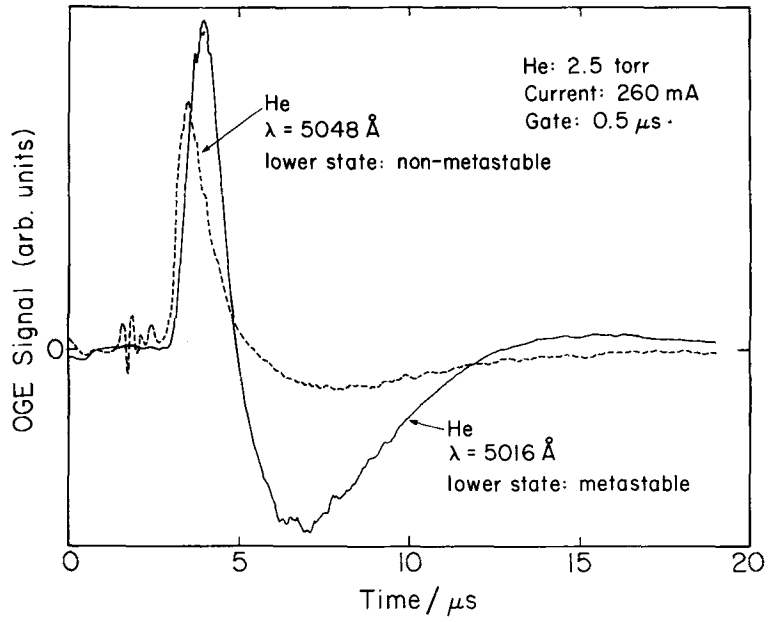

(*a*)

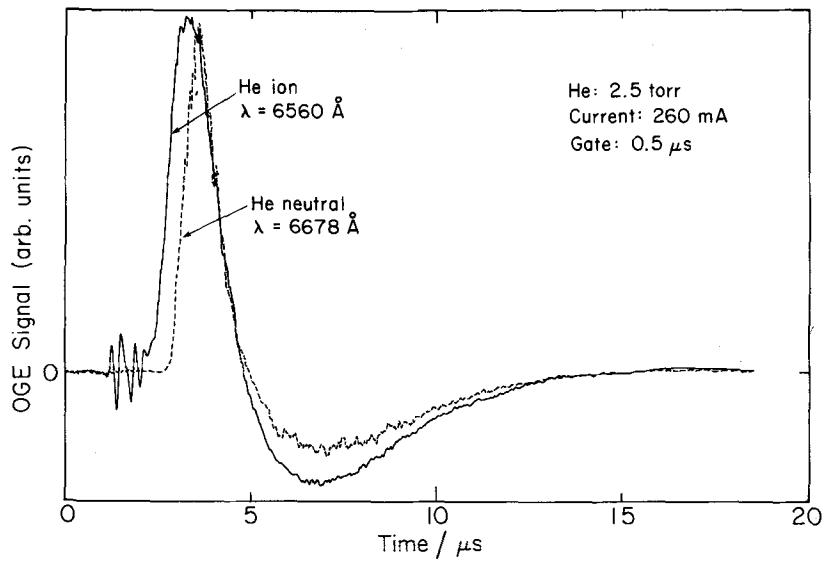

(*b*)

Figure 5. Time dependences of different types of OGE signals, as measured with a boxcar integrator after pulsed laser excitation. (*a*) Comparison of an OGE signal originating in a non-metastable state of He with one from a metastable state. (*b*) Comparison of an OGE signal from He^+ with that from neutral He (non-metastable).

at $\sim 10\ \mu s$ was often observed. The implications of these different time dependences are discussed later in this paper.

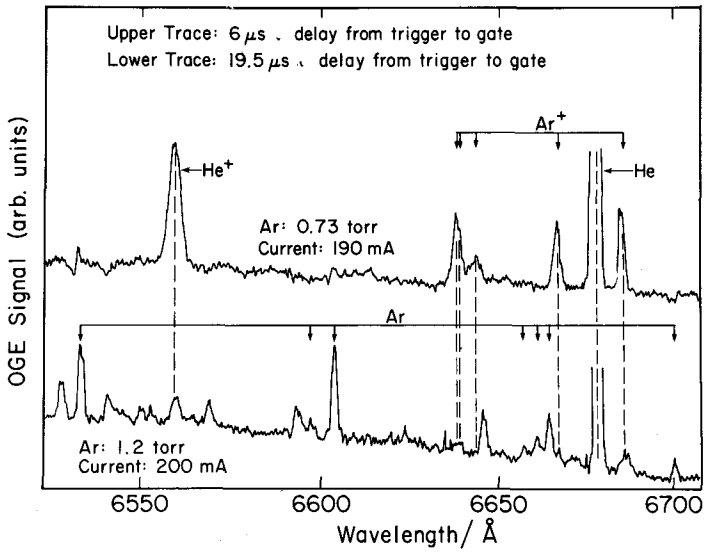

Figure 6. Optogalvanic spectra of Ar. The difference in the time dependences of OGE signals of neutral species relative to those from ionic species is utilized to separate their spectra. Upper trace : boxcar gate was set 6 μs after the triggerpulse for the laser. Lower trace : boxcar gate was set 19·5 μs after the triggerpulse for the laser.

3.2. *Molecular spectra*

Electronic spectra of several molecules (table 3) were detected with the same methods as used to obtain the atomic spectra discussed above. The $B\ ^3\Pi_g$–$A\ ^3\Sigma_u^+$ (First Positive) system of N_2 was observed from 5845 Å to 6190 Å in pure N_2 and N_2/He discharges at pressures from 1–4 torr and currents of 100–400 mA. The $c_4\ ^1\Pi_u$–$a''\ ^1\Sigma_g^+$ (Ledbetter) system at ~ 5977 Å was also observed. From the relative intensities of the various bands observed in the First Positive System, the vibrational temperature for the $A\ ^3\Sigma_u^+$ state was estimated to be $T_v(A) \cong 2200$ K and was independent of discharge conditions over the range studied here. A portion of the N_2 spectrum obtained with the cw dye laser is shown in figure 7. It was noticed that the sign of the laser-induced impedance change appears opposite for different transitions. As noted by Feldman [19], predissociation in the $B\ ^3\Pi_g$ state of N_2 occurs from levels with $v \geqslant 12$; transitions to these levels deplete the discharge of electron-producing excited states and probably explain the observed increase in discharge impedance upon laser excitation of these vibrational bands. However, one must be cautioned that when using phase-sensitive detection with the OGE it is possible that the phase of the lock-in is optimum for certain signals but not for others and that for some transitions it is peaked for a portion of the plasma response which corresponds to an opposite voltage change (see pulsed laser time dependence measurements). Since it is the time average of the plasma response

that is actually measured, signals with differing time dependences can appear with opposite sign after lock-in processing.

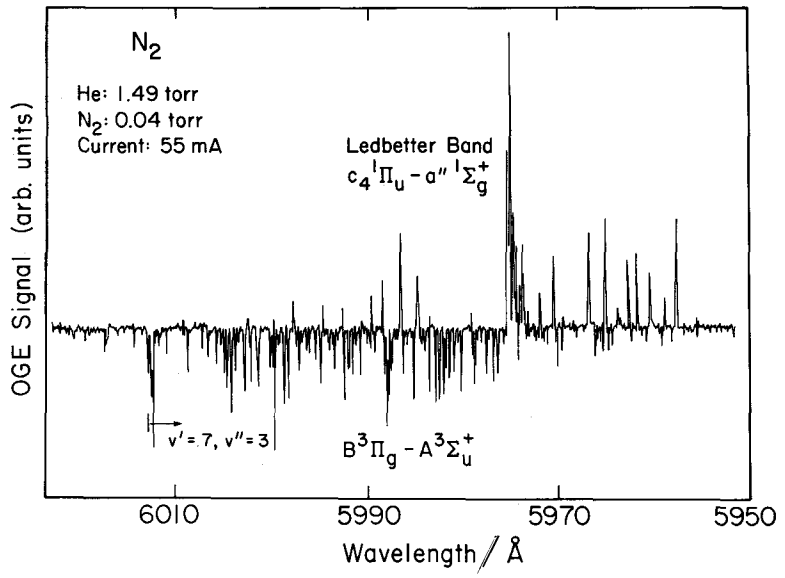

Figure 7. A part of the extensive OGE spectrum of N_2 is shown, including the (7, 3) band originating in the lowest metastable triplet state ($A\ ^3\Sigma_u^+$) and the Ledbetter band, originating in the Rydberg state $a''\ ^1\Sigma_g^+$.

The ring dye laser, when operated with the unidirectional device and birefringent filter but no intracavity etalon, provided a resolution of 0·1 cm^{-1}. However, due to the scanning characteristics of the laser, wavelength assignments were limited to an accuracy of $\sim 1\ cm^{-1}$. It was observed that the relative position of Ne calibration lines shifted by as much as 35 GHz in consecutive scans and, as evidenced by monitoring the laser output with a 20 GHz spectrum analyser, this coincided with mode-hopping of the laser. Consequently, exact rotational assignments of very dense spectra, such as those of N_2 in figure 7, were difficult to make with this system.

The $^2A_1$–$^2B_1$ system of NH_2 (in the region from 5700 Å to 6200 Å) was observed in hydrogen discharges containing trace impurities of N_2 (figure 8). Transitions to Σ, Δ and Γ vibronic levels of the 0, 9, 0 band and Π and Φ levels of the 0, 10, 0 band, as listed by Dressler and Ramsay [20], were observed. These spectra increased in intensity upon the addition of N_2 to the discharge, being strongest with a few per cent N_2 in $\sim$2·5 torr H_2 at currents of $\sim$500 mA. Due to the shortness of the rotational progressions observed and the poor scan characteristics of the laser, rotational temperatures could not be extracted for these spectra.

In pure H_2 discharges, very weak transitions were observed in the $i\ ^3\Pi_g$–$c\ ^3\Pi_u$ system of H_2 in the region from $\sim$5830–6050 Å. Typical discharge conditions were 1 torr H_2 and 150 mA discharge current.

Two bands, at $\sim$6059 and $\sim$6165 Å, were observed in mixtures of N_2/He and H_2/He under very different discharge conditions. These were subsequently

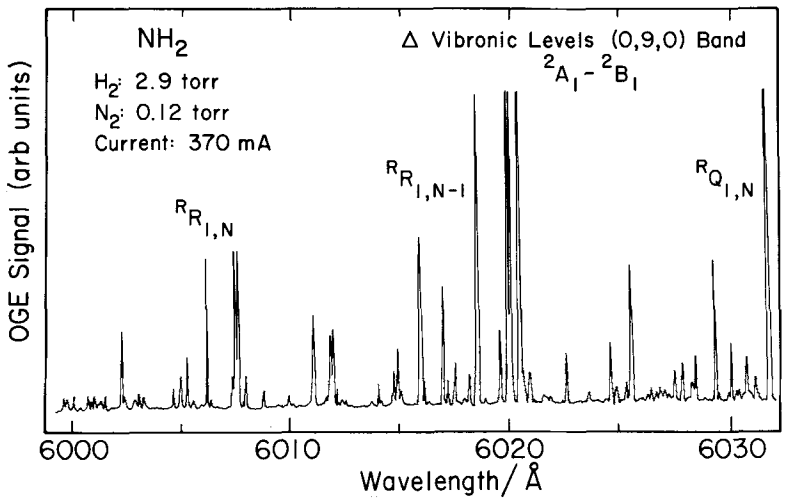

Figure 8. A part of the OGE spectrum of NH_2, excited with a cw ring dye laser. NH_2 is formed in a discharge of hydrogen containing trace amounts of nitrogen.

assigned to the $A\ ^2\Sigma^+$–$X\ ^2\Pi_{3/2,1/2}$ transition of CuO((0, 0) and (1, 1) bands) [21]. Observation of this system indicates the possible application of optogalvanic spectroscopy to the investigation of metal-containing molecules generated in a discharge by sputtering metal from an appropriate cathode. It is possible that the metal oxide was sputtered directly from the cathode surfaces or that it was generated from sputtered Cu atoms and impurity levels of oxygen. Optimum conditions for observing CuO were not determined, but it was detected in discharges of 1·5 torr He/0·02 torr N_2 and currents of 330 mA , and also in a mixture of 9·2 torr He and 0·025 torr H_2 with 700 mA current. In the latter case spectra of NH_2 were also observed, indicating the presence of other contaminating gases.

Several molecular bands originating in the $b\ ^3\Pi_g$ state of He_2 were observed in the region between 5680 and 6050 Å in discharges of pure helium at ~ 10 torr and 300 mA. These bands (figure 9) were assigned [22] to the electronic transitions $f\ ^3\Sigma_u^+$–$b\ ^3\Pi_g$, $f\ ^3\Pi_u$–$b\ ^3\Pi_g$, and $f\ ^3\Delta_u$–$b\ ^3\Pi_g$ (table 3). There are two major channels for the production of He_2 in the plasmas used here :

(i) Three-body He metastable recombination

$$He^* + 2He(1s) \rightarrow He_2^* + He(1s) + \Delta E.$$

(ii) Recombination of He_2^+ molecular ions

$$He_2^+ + e^- + M(\text{electron, } He(1s)) \rightarrow He_2^* + M + \Delta E.$$

The observation of Rydberg spectra of He_2 lends credibility to the idea of developing OGE into a general method for obtaining spectra of molecules with repulsive ground states by generating them ' from the top down '. This is especially indicated by the fact that our observed He_2 spectra originate in the $b\ ^3\Pi_g$ state, which cannot be formed directly by the metastable recombination process. (It should be noted that both the $a\ ^3\Sigma_u^+$ and $A\ ^1\Sigma_u^+$ states directly formed by process 1 have lower energies than the $b\ ^3\Pi_g$ state). Intensities of

individual rotational lines were measured in an effort to characterize the rotational temperature of this species. The interesting results of these measurements will be discussed in the next section.

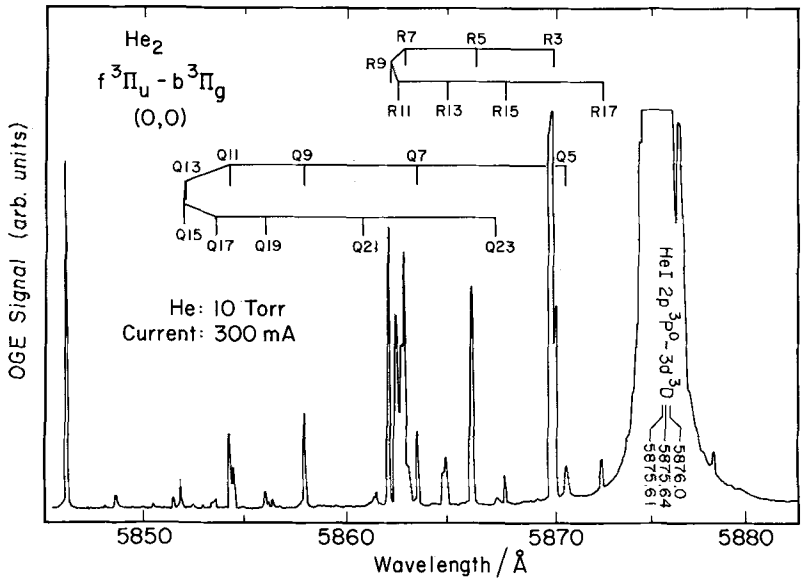

Figure 9. The OGE spectrum of He_2 originating in the non-metastable Rydberg state ($b\,^3\Pi_g$). Atomic He lines at 5876 Å (unresolved) are also shown. The atomic He lines near 5876 Å are at least two orders of magnitude stronger than the molecular lines. A cw ring dye laser was used for the excitation.

The $d\,^3\Delta_i$–$a\,^3\Pi_r$ (3, 0), (4, 1), and (7, 0) vibrational bands of CO were detected from (6380 Å–6670 Å) and from (5030 Å–5145 Å) in He discharges containing a few per cent CO at total pressures near 3 torr and discharge currents of 250 mA. The spectrum of the (3, 0) band (figure 10) consists of 27 rotational branches, each with approximately 18 lines in the range between 15 625 cm^{-1} and 15 220 cm^{-1}. This gives a density of about 1 line/cm^{-1}. With the laser bandwidth of 3 cm^{-1} it was impossible to revolve single rotational lines. Only a few intense bandheads could be assigned unambiguously.

Finally, the $A\,^2\Pi$–$X\,^2\Sigma^+$ system of CN was observed over the range from 5480–6220 Å and from 6400–6820 Å in a mixture of a few per cent C_2N_2 in He at pressures of 1·3 torr and currents of 150 mA.

Of these molecular spectra, the N_2, NH_2, and H_2 systems have previously been observed with OGE detection by Feldman [19] in a DC positive column discharge and by Suzuki [23] in an RF plasma. In those studies NH_2 was observed in discharges of NH_3, whereas in the present case it was seen in mixtures of N_2 and H_2 as discussed. The CuO, He_2, CO, and CN data represent the first detections of these molecules by OGE.

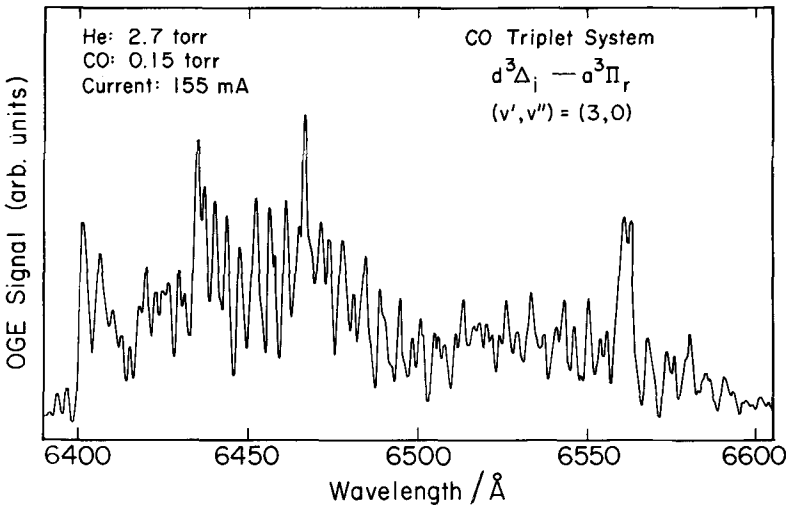

Figure 10. The (3, 0) band of CO originating in the lowest metastable triplet state ($a\,^3\Pi_r$), excited with a pulsed dye laser, is shown. The rotational structure is unresolved due to the $\sim 3\ \mathrm{cm}^{-1}$ band width of the CMX-4 laser.

4. Discussion

4.1. *Time dependence and kinetics*

The complexity of the time-resolved OGE signals seen in figure 5 clearly indicates that several kinetic processes are involved in effecting a laser-induced change in the plasma impedance. The impedance first decreases upon laser excitation of a transition (positive OGE signals in figure 5 correspond to a decrease in impedance, or an increase in the current) then increases, and finally decreases again, in some cases below the steady-state value, before asymptotically returning to steady-state conditions. This behaviour can be qualitatively explained as follows : the laser creates a non-equilibrium excited state population which can perturb the plasma through a number of different processes. A change in plasma impedance will occur when these processes either change the charged particle density or mobility. The specific processes which must be considered are :

(i) Electron impact ionization :
$X^* + e^- \rightarrow X^+ + 2e^-$.

(ii) Superelastic collisions :
$X^* + e^-(\text{thermal}) \rightarrow X + e^-(E \gg \text{thermal})$.

(iii) Associative ionization :
$X^* + X \rightarrow X_2^+ + e^- + \Delta E$
(ΔE is usually small because the dimer ion is formed with highest probability in a rotation–vibration state nearly resonant with the excitation energy).

(iv) Penning ionization :
$X^* + Y^*(\text{metastable}) \rightarrow X^+ + Y + e^- + \Delta E$.

(v) Cathode photoemission :
$X^* \rightarrow X + h\nu$
$h\nu + M \rightarrow e^- + \Delta E$.
If the energy of the photon is higher than the work function of the cathode material, an electron can be created by photoemission.)

Laser-induced changes in recombination rates, charge exchange, or ion-molecule reactions have not yet been considered in this model because molecular ion spectra have not yet been observed, and these processes are expected to be of secondary importance for the studies of the neutral species discussed here.

In the negative glow region of a discharge the current is carried principally by electrons, although the ion density is nearly the same, because the electron mobility is much higher than the ion mobility. The production of additional electrons from ionization of the excited states populated by the laser, as well as the increased production of *fast* electrons through superelastic collisions of slow (thermal) electrons with these excited states, *decreases* the plasma impedance during the exciting laser pulse. Immediately following termination of the laser pulse the plasma experiences a decrease in the excited state populations, relative to steady-state conditions. The laser excitation has, in effect, caused a trade-off : the steady-state population of plasma-excited states for the momentarily increased plasma conductivity, from ionization and superelastic collisions. These processes in turn, convert the laser-excited states to ground state species and thereby decrease the density of plasma excited states. The excited state population serves as an energy reservoir for the electron gas, coupled through superelastic collisions. Decreasing the density of plasma excited states will cause a decrease in the average electron temperature, thus lowering the electron drift velocity and hence raising the plasma impedance. This is the origin of the negative part of the OGE signal, which corresponds to the increase in impedance following the initial fast positive signal.

The excess ions produced during the laser pulse have no significant impact on the discharge impedance until they drift into the cathode fall region, where they are accelerated into the cathodes. The fast rise of the negative portion of the OGE signal, which sometimes leads to a second positive signal, is most likely due to the contribution of the excess ions produced by the laser.

The perturbation in excited state population density caused by the laser will return to equilibrium with a time constant characteristic for the respective state. When this perturbation is small compared with the total population in the reservoir (lower) state, the temporal behaviour can be described by a single rate equation,

$$\dot{n}_1 = -\gamma_1 n_1 + \gamma_0 n_0, \tag{2}$$

where n_1 is the population in the state perturbed by the laser, n_0 is that in the reservoir state for populating n_1, and γ_1, γ_0 are the loss rates.

If n_0 is not significantly changed by the laser, the solution of (1) is

$$n_1 = n_1(0) \exp(-\gamma_1 t) + \frac{\gamma_0}{\gamma_1} n_0. \tag{3}$$

Defining Δn to be the change induced by the laser at the time $t = 0$ then we have

$$n_1 = -\Delta n_1 \exp(-\gamma_1 t) + \frac{\gamma_0}{\gamma_1} n_0. \tag{4}$$

This shows that after the perturbation, the population n_1 returns to the equilibrium value $(\gamma_0/\gamma_1)n_0$ with a time constant of $1/\gamma_1$. It means that longer-lived excited states take longer to recover from a perturbation. As we will see later, for the case of metastable He, the collisional loss rate is on the order of 10^3 s^{-1}.

We shall now discuss the relative importance of the processes involved in the maintenance of the discharge. The current density is mainly due to electrons in the negative glow region :

$$j = e n_e v_d. \tag{5}$$

Changing either the electron density (n_e) or the electron drift velocity (v_d) will result in a change in discharge current. The fractional change can be written as

$$\frac{dj}{j} = \frac{dn_e}{n_e} + \frac{dv_d}{v_d}. \tag{6}$$

The contribution due to electron–ion pair production is given by

$$\frac{dj}{j} = \frac{1}{n_e} \text{ (ion contribution neglected).} \tag{7}$$

Superelastic processes, in which the electron receives the excitation energy of the atom or molecule, will raise the electron temperature. The increase in the energy density of the electron gas is :

$$\frac{dE}{E} = \frac{E_{exc}}{E(\text{thermal})n_e} = \frac{E_{exc}}{3/2\, kT_e n_e}. \tag{8}$$

The excitation energy is transferred in a superelastic collision to kinetic energy of the electron, which subsequently will raise the electron temperature as this fast electron is thermalized. This thermalization occurs on a nanosecond time scale under the conditions used in our experiment [11], and the change in electron temperature is

$$\frac{dT_e}{T_e} = \frac{dE}{E}. \tag{9}$$

The electron drift velocity depends upon the electron temperature [24]

$$v_d \sim (T)^{3/4}. \tag{10}$$

This leads to a fractional change in current density due to electron gas heating :

$$\frac{dj}{j} = \frac{dv_d}{v_d} = \frac{3}{4} \frac{E_{exc}}{3/2\, kT_e} \frac{1}{n_e}. \tag{11}$$

Comparing (11) with (7) shows that electron gas heating has a larger effect on the plasma than electron-ion pair production when $3/4\ (E_{exc}/3/2\, kT_e) > 1$. All of the processes previously mentioned can influence the plasma impedance by either or both of these mechanisms. These collisional processes, however, have to compete with the radiative decay of the excited levels in order to create an OGE signal. We will discuss the collision rates for the specific case of the helium $2s\ ^1S$–$3p\ ^1P^0$ transition at 5016 Å.

(i) *electron impact ionization*

The cross sections for excited state ($n \geqslant 3$) ionization by electron impact are unknown. However, this cross section scales [25] as

$$\sigma_{\text{ion}}(n, l) \sim \frac{1}{IP(n, l)}; \tag{12}$$

Using the cross section [11] $\sigma_{\text{ion}}(1s) = 5 \times 10^{-17}$, we obtain the estimate $\sigma_{\text{ion}}(3p) \sim 8 \times 10^{-16}$ cm^2. The kinetic energy of thermal electrons in our discharge is approximately 1000 K. With the $IP(3p) = 12\,106$ cm^{-1} we obtain a Boltzmann factor at $\sim 6 \times 10^{-6}$. The density of *non-thermal* electrons with sufficient energy to ionize the $3p$ state, however, is only two orders of magnitude lower than the thermal electron density [11]. We have measured n_e(thermal) $\sim 1{\cdot}5 \times 10^{11}$ cm^{-3}. The ionization rate due to the non-thermal electrons is :

$$n_e(1{\cdot}5 \text{ eV})\sigma_{\text{ion}}(3p)\overline{V}_{\text{rel}} \approx 100 \text{ s}^{-1}.$$

(ii) *Superelastic collisions*

The cross sections for superelastic collisions are related to the cross sections for electron impact excitation by the Klein–Rosseland formula [25]

$$\sigma_{ji}(\Delta E) = \sigma_{ij}(E_j - E_i + \Delta E)\frac{g_i}{g_j}\frac{E_j - E_i + \Delta E}{\Delta E}. \tag{13}$$

where E_i, E_j represent the energy of lower, upper states, ΔE is the energy of thermal electrons, and g_i, g_j are degeneracy factors. The electron impact excitation cross section for the $3p\ ^1P$ state is known [26] :

$$\sigma_{ij}(187\,000 \text{ cm}^{-1}) = 3{\cdot}5 \times 10^{-18} \text{ cm}^2.$$

This yields $\sigma_{ji} \approx 3 \times 10^{-16}$ cm^2. The rate for superelastic collisions is given by

$$n_e(\text{thermal})\overline{V}_{\text{rel}}\sigma_{ji} \approx 900 \text{ s}^{-1}.$$

(iii) *Associative ionization*

The cross section for this process has been measured [27] for all $n = 3$ states and

$$\sigma(3\ ^1P) = 3{\cdot}1 \text{ Å}^2.$$

The He ground state density is typically 5×10^{16} cm^{-3} in our experiment and the neutral gas temperature is approximately the cathode temperature (300 K). The rate for associative ionization is then

$$n_{\text{He}}\overline{V}\sigma(3\ ^1P) = 3 \times 10^6 \text{ s}^{-1}.$$

(iv) *Penning ionization*

This process is energetically possible only when both He atoms are in an excited state. Because the metastable density is the highest among all of the excited states, the reaction He* (metastable) + He($3\ ^1P$) $\rightarrow$ He$^+$ + He + e$^-$ + ΔE is the dominant Penning process for the He($3\ ^1P$) state. Because the metastable density is about 4–5 orders of magnitude below that of the ground state [11, 25], the rate can be expected to be small compared with associative ionization, although the measured cross section for the metastable–metastable Penning ionization is comparatively high [28] :

$$\sigma(2s) \approx 85 \text{ Å}^2.$$

For $n_{He(2s)} \sim 5 \times 10^{12}$ cm^{-3} we obtain a rate of $8{\cdot}5 \times 10^{3}$ s^{-1} for Penning ionization of the metastable state. Although the cross section for $n=3$ is not known, it is reasonable to assume that they do not differ substantially.

(v) *Photoelectric effect*

The $3p\,^1P$ state radiatively decays to $1s\,^1S$ and $2s\,^1S$ at 537 Å ($A = 5{\cdot}66 \times 10^{8}$ s^{-1}) and 5016 Å ($A = 1{\cdot}34 \times 10^{7}$ s^{-1}) respectively. It has to be considered that for transitions to the ground state the plasma is optically thick at the pressures used here. The mean free path of the photon can be calculated as follows:

$$\text{Mean free path} = \frac{1}{n_{He} \cdot \sigma_{abs}}.$$

With

$$\sigma_{abs} = \left(\frac{\lambda^2}{8\pi}\right)\frac{A}{\Delta\nu} \tag{14}$$

and

$$\Delta\nu_{Doppler} = \frac{\nu}{c}(8\,kT\,ln\,2/m)^{1/2}. \tag{15}$$

The mean free path for a 537 Å photon is $\sim 1 \times 10^{-3}$ cm and 2·7–0·5 cm for a 5016 Å photon assuming the density of He($2s\,^1S$) to be $1\text{–}5 \times 10^{12}$ cm^{-3}. The ratio of the A values ($A_{537}/A_{5016} \sim 42$) implies that an excited $3P\,^1P^0$ atom will emit a 537 Å photon and reabsorb it 42 times before it will emit a 5016 Å photon. The excited state therefore (statistically) ' travels ' a total distance of 42 times 1×10^{-3} cm before it decays through the 5016 Å channel. If the laser photon is absorbed close to the cathode surface the 537 Å photons can hit the cathode and cause the emission of an electron, thus contributing to the OGE, particularly because these photoelectrons will be amplified in the cathode fall region.

The lifetime of the excited state is mainly given by the decay via the 5016 Å channel because the 537 Å channel is optically thick. This means that the radiative decay rate is $1{\cdot}34 \times 10^{-7}\ s^{-1}$.

Of all the collisional processes discussed, associative ionization is the most effective for competition with radiative decay. 20 per cent of the $3p\,^1P^0$ population will not be lost through associative ionization. Using this fact and equation (7) with $n_e = 2 \times 10^{11}$ cm^{-3} the fractional change in current density per absorbed 5016 Å laser photon is

$$\frac{dj}{j} \approx 1 \times 10^{-12}/\text{photon}.$$

The noise level in a pure He discharge as measured by the voltage drop across a 100 Ω ballast resistor at 500 mA discharge current typically is 0·5 μV (lock-in at 5 kHz). This means that a fractional change in total current of 10^{-8} will be detected with a signal to noise ratio of one. If the laser excited volume equals the discharge volume a total current change of 10^{-8} can be achieved by the absorption of 10^{4} photons.

Other ionizing processes are not very important for the OGE as far as electron-ion pair production is concerned because their rates are several orders of magnitude smaller than that of associative ionization. However, processes

like Penning ionization and superelastic collisions, for example, release a high amount of excess energy to the electron. The excess energy in a Penning ionization $He^*(2s)+He^*(3p)\rightarrow He^+ + e + He$ is $\sim 150\,000\ cm^{-1}$. Due to the factor $(3/4\ E_{exc})/(3/2\ kT_e)$ in equation (11) one such collision has about 100 times more effect on the discharge due to electron gas heating than the production of electron–ion pairs.

In order to establish a detailed model for the OGE one has to know the collisional rates of both upper and lower states. If, for example, the cross section for Penning ionization of the $2s\ ^1S$ were negligible as compared with the $3p\ ^1P^0$ state then the total excess energy of 150 000 cm^{-1} would contribute to an opto-galvanic signal. If the cross sections were equal however, only the photon energy would contribute to the OGE because with or without absorption the He* atom would undergo a Penning collision with the same probability. The only difference is that with the absorption the additional energy of the photon is deposited in the electron gas. This shows that in suitable cases, where the absorption of a photon opens or closes very energetic channels, the effect on the plasma can be tremendous. This explains the observed fact that OGE is a very sensitive method to study molecules in excited states.

Laser excitation of the previously mentioned He $n=2\rightarrow n=3$ transitions at 5875 and 6678 Å opens the channel for associative ionization. The $n=2$ states ($E<171\ 130\ cm^{-1}$) lie below the energy necessary for associative ionization ($IP(HeI)-D_0(He_2^+)=179\ 236\ cm^{-1}$) while the $n=3$ states ($E>183\ 230\ cm^{-1}$) lie above the energy threshold. These lines consequently exhibit extraordinarily strong OGE signals. The 5048 Å line originating in the same lower state as the 6678 Å line exhibits a weaker OGE signal (normalized to the oscillator strength) because the cross-section for associative ionization of the upper state $4s\ ^1S$ is small.

4.2. *He_2 rotational populations distribution*

In figure 11 the intensity of He_2 rotational lines divided by the Hönl–London factors is plotted logarithmically versus $K(K+1)$ in order to evaluate the population distribution of the rotational levels. The Hönl–London factors were corrected for *l*-uncoupling [29]. The observed non-linear plot indicates that the rotational population distribution is non-Boltzmann, hence we cannot assign a unique rotational temperature. The He_2 molecules are formed either by three-body recombination of metastable He or by electron–ion recombination; processes, which leave the He_2 molecules in non-equilibrium rotation–vibration states. One would expect that the He_2 rotational distribution will thermalize in collisions with neutrals (the most abundant species in the discharge) to translational temperature. The temperature of neutrals is found to be ~ 300 K in the hollow-cathode discharge used here [11]. For low rotational quantum numbers ($K\leqslant 8$) we observe a fast drop in intensity corresponding to a temperature of 300 K. Above K = 8 a change of curvature occurs and the decrease in intensity with J is substantially slower. We attribute this to the fact that He_2 ($b\ ^3\Pi_g$) has a large B value of 7·447 cm^{-1}, hence R–T transfer in collisions with neutrals becomes inefficient as the rotational energy level spacings become larger than the translational energy of the neutrals. Theory and experiments indicate a symmetry-induced selection rule for rotational transitions in homonuclear molecules by collisions [30] of $\Delta K=\pm 2,\ \pm 4$. The $K=8\rightarrow 10$

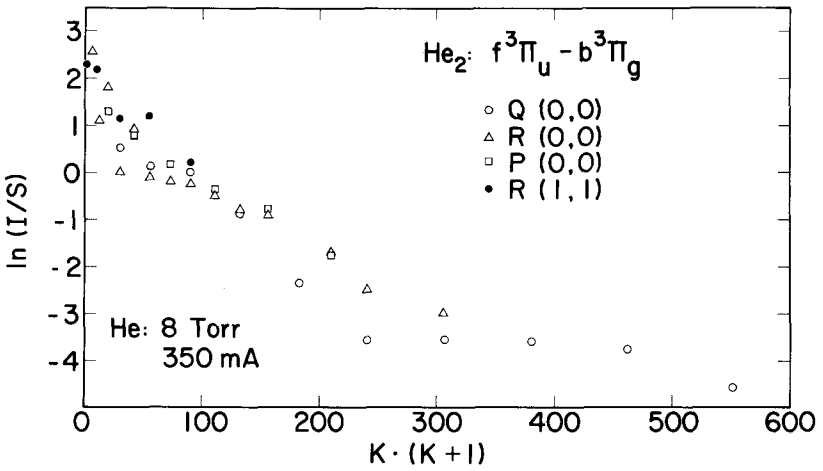

Figure 11. The intensity of He_2 rotational lines, normalized to modified Hönl–London factors S^* (l-uncoupling [29]), is plotted versus $K(K+1)$ to obtain the population distribution of the rotational energy levels.

transition corresponds to $\Delta E = 280\ cm^{-1}$, while the translational energy (kT) at 300 K is $\sim 200\ cm^{-1}$. R–T relaxation through collisions with neutrals thus becomes inefficient for $K \geqslant 8$. Collisional relaxation and excitation of rotating He_2 molecules by thermal electrons become more important at this point. The electron temperature (T_e) is known to be ~ 1000 K. The slope of the curve for K between 8 and 17 yields a rotational ' temperature ' of ~ 800 K, corresponding to an energy of $\sim 560\ cm^{-1}$. For $K \geqslant 18$ ($K(K+1) \geqslant 340$) the rotational spacing for $\Delta K = 2$ becomes larger than the thermal electron kinetic energy. The decrease in intensity above $K = 18$ consequently levels off because collisions with electrons then become inefficient at relaxing these high rotational states. Rotational lines with K values as high as 23 have been observed in this work. The energy of a rotational level with $K = 23$ is $\sim 4050\ cm^{-1}$. Conservation of energy and angular momentum makes it very unlikely that He_2 is formed in these highly excited rotational states because neither the neutral atoms involved in three-body recombination nor the electrons and ions involved in electron–ion recombination have sufficient angular momentum. Non-thermal electrons with sufficient energy do not carry enough angular momentum to excite He_2 ($K \geqslant 20$) rotations. However, vibrational–rotational energy transfer of the type

$$He_2(v_1, K_1) + He_2(v_2, K_2) \rightarrow He_2(v_1^{-1}, K'_1) + He_2(v_2, K'_2)$$

is known to be an efficient channel for vibrational relaxation of light molecules, if the rotational energy becomes larger than the translational energy [31–33]. Therefore the most likely mechanism for rotational heating of He_2 up to $K = 23$ is vibrational–rotational energy transfer of the above type. For the intermolecular vibrational–rotational energy transfer the values for K_1, K'_1, K_2, and K'_2 can always be chosen to make this process nearly energy resonant, and probable as far as angular momentum transfer is concerned. In addition there is reason to believe that the He_2 density in the centre of a hollow cathode discharge at 4 torr and 500 mA is higher than the corresponding density of high energy electrons.

5. Summary

In this work we have investigated the optogalvanic effect for Ar, He, Ne, Ar^+, He^+, Cu, and Na atoms and the N_2, H_2, CO, CN, NH_2, He_2, and CuO molecules in recombination-limited hollow cathode plasmas.

Comparative studies of the time dependences of neutral He transitions originating in metastable and non-metastable levels with those of He^+ transitions suggests a general mechanism for the OGE in which laser-excited states first produce an increase in conductivity through enhanced electron impact ionization, superelastic collisions, or enhanced associative ionization ; a decrease in conductivity then results, caused by electron cooling from an increased density of low-quantum state species produced in the initial step. A second increase in conductivity is sometimes observed at later times, due to the effects of altered ion densities, that in turn result from the initial step on the plasma impedance. The initial increase in conductivity occurs somewhat earlier for ions than for neutrals, as a result of increased cross-sections for collisional deactivation of the excited states. The different time dependence was utilized to substantially enhance the intensities of optogalvanic electronic spectra of He^+ and Ar^+ ions, relative to those of neutral species.

It was shown that the linewidths of atomic Rydberg series extending to high n can be used to provide a convenient measurement of the plasma density in these systems. Autoionizing transitions in Cu(I) were observed to produce strong OGE signals. It is suggested that measurement of the linewidths of such autoionizing transitions will, in turn, provide a way to measure the very fast autoionization rates, which are otherwise difficult to study. A continuous background OGE signal was observed in all of the cases examined here, probably resulting from direct ionization of high Rydberg levels of species excited in the plasma. It was found that as carbon deposited on the cathodes was vaporized with the pulsed laser, the discharge voltage could be switched essentially to zero.

It was demonstrated that the OGE can be a general method to investigate transitions originating in metastable states of molecules ($A\ ^3\Sigma_u^+$ of N_2, $a\ ^3\Pi$ of CO, $c\ ^3\Pi_u$ of H_2). This could be useful in studying high multiplicity systems that are difficult to observe by emission or absorption spectroscopy (e.g. quartet systems of CH). Moreover, because the OGE is generally very sensitive to the *dissociation* channels of molecules excited in the plasma, optogalvanic spectroscopy is complimentary to direct emission and absorption techniques for species which undergo rapid predissociation. The study of He_2 presented here further indicates exciting possibilities for carrying out spectroscopic experiments or molecules generated ' from the top down ' in recombination plasmas. This could prove particularly valuable for species like H_3 or NH_4 which have repulsive ground-state potential surfaces and excited states which predissociate. The observation of CuO and Cu(I) OGE spectra suggests that optogalvanic spectroscopy might also be useful for investigation of metal-containing species, with the metal being produced through ion sputtering from a suitable cathode material.

An examination of the various processes that occur in plasma environments indicates that associative ionization and autoionization are effective means for coupling laser energy into the plasma besides direct electron impact ionization. Measurement of intensities of rotational lines of He_2 indicates a high degree of non-equilibrium among the rotational states, and suggests that both electron–

rotation and vibration–rotation energy transfer processes become important for high J states of light molecules in such plasmas.

This work was principally supported by the National Science Foundation (Grant No. CHE 8207307), with partial support from the Dreyfus Foundation and the Research Corporation. J. P. thanks the Chemical Manufacturer's Association for postdoctoral support. The lasers were borrowed from the San Francisco Laser Center, supported by the National Science Foundation under Grant No. CHE79-16250 awarded to the University of California at Berkeley in collaboration with Stanford University. We wish to acknowledge Dr. B. Warner for many helpful comments and suggestions.

References

[1] Turk, G. C., Mallard, W. G., Schenck, P. K., and Smyth, K. C., 1979, *Analyt. Chem.*, **51,** 2408, and references therein.
[2] Skolnick, M. L., 1970, *I.E.E.E. Jl quant. Electron.*, **6,** 139. Green, R. B., Keller, R. A., Luther, G. C., Schenck, P. K., and Travis, J. C., 1977, *I.E.E.E. Jl quant. Electron.*, **13,** 62.
[3] Ausschnitt, C. P., Bjorklund, G. C., and Freeman, R. R., 1978, *Appl. Phys. Lett.*, **33,** 851.
[4] Goldsmith, J. E. M., and Lawler, J. E., 1981, *Contemp. Phys.*, **22,** 235, and references therein.
[5] Webster, C. R., and Rettner, C. T., 1983, *Laser Focus*, **19,** 41, and references therein.
[6] Miron, E., Smilanski, I., Liran, J., Lavi, S., and Erez, G., 1979, *I.E.E.E. Jl quant. Electron.*, **15,** 194.
[7] Saykally, R. J., Begemann, M. H., and Pfaff, J., 1981, *Proceedings of the Fifth International Conference on Laser Spectroscopy*, edited by A. R. W. McKellar, T. Oka and B. P. Stoicheff (Springer Series in Optical Sciences).
[8] Herzberg, G., 1979, *J. chem. Phys.*, **70,** 4806.
[9] Herzberg, G., and Hougen, J. T., 1983, *J. molec. Spectrosc.*, **97,** 430.
[10] Warner, B. E., Gerstenberger, D. C., Reid, R. D., McNeil, J. R., Solanki, R., Persson, K. B., and Collins, G. J., 1978, *I.E.E.E. Jl quant. Electron.*, **14,** 568.
[11] Warner, B. E., 1979, Ph.D. Thesis, University of Colorado.
[12] Griem, H. R., 1974, *Spectral Line Broadening by Plasmas* (Academic).
[13] Shenstone, A. G., 1948, *Phil. Trans. R. Soc.* A, **241,** 297.
[14] Allen, C. W., 1932, *Phys. Rev.*, **39,** 42, 55.
[15] Vasudev, R., and Zare, R. N., 1982, *J. chem. Phys.*, **76,** 5267.
[16] Schenck, P. K., and Smyth, K. C., 1978, *J. opt. Soc. Am.*, **68,** 626.
[17] Keller, R. A., Engleman, R., Jr., and Zalenski, E. F., 1979, *J. opt. Soc. Am.*, **69,** 738.
[18] Rettner, C. T., Webster, C. R., and Zare, R. N., 1981, *J. chem. Phys.*, **85,** 1105.
[19] Feldmann, D., 1979, *Optics Commun.*, **29,** 67.
[20] Dressler, K., and Ramsay, D. A., 1959, *Phil. Trans. R. Soc.* A, **251,** 553.
[21] Appleblad, D., and Lagerqvist, A., 1974, *Physica scripta*, **10,** 307.
[22] Ginter, M. L., 1965, *J. molec. Spectrosc.*, **18,** 321.
[23] Suzuki, T., 1981, *Optics Commun.*, **38,** 364. Suzuki, T., and Kakimoto, M., 1982, *J. molec. Spectrosc.*, **93,** 423.
[24] Engel, A. v., 1965, *Ionized Gases* (Oxford University Press).
[25] Delcroix, J. L., Ferreira, C. M., and Ricard, R., 1976, *Principles of Laser Plasmas*, edited by G. Bekefi (Wiley–Interscience).
[26] St. John, R. M., Miller, F. L., and Lin, Ch. C., 1964, *Phys. Rev.*, **134,** A888.
[27] Wellenstein, H. F., and Robertson, W. W., 1972, *J. chem. Phys.*, **56,** 1077.
[28] Deloche, R., Monchicourt, P., Cheret, M., and Lambert, F., 1976, *Phys. Rev.* A, **13,** 1140.
[29] Kronig, R. de L., and Fujioka, Y., 1930, *Z. Phys.*, **63,** 175.

[30] LEVINE, R. D., and BERNSTEIN, R. B., 1974, *Molecular Reaction Dynamics* (Oxford University Press).
[31] MILLIKAN, R. C., and OSBURG, L. A., 1964, *J. chem. Phys.*, **41**, 2196.
[32] MOORE, C. B., 1965, *J. chem. Phys.*, **43**, 2979.
[33] CHEN, M. Y.-D., and CHEN, H.-L., 1972, *J. chem. Phys.*, **56**, 3315.